

Article

Multi-Objective Constructral Design for Quadrilateral Heat Generation Body with Vein-Shaped High Thermal Conductivity Channel

Hongwei Zhu ^{1,2,3}, Lingen Chen ^{1,2,3,*} , Yanlin Ge ^{1,2,3}, Shuangshuang Shi ^{1,2,3} and Huijun Feng ^{1,2,3}

¹ Institute of Thermal Science and Power Engineering, Wuhan Institute of Technology, Wuhan 430205, China

² Hubei Provincial Engineering Technology Research Center of Green Chemical Equipment, Wuhan 430205, China

³ School of Mechanical & Electrical Engineering, Wuhan Institute of Technology, Wuhan 430205, China

* Correspondence: lingenchen@hotmail.com

Abstract: Based on the quadrilateral heat generation body (HGB) proposed by previous literature, the multi-objective constructral design is performed. Firstly, the constructral design is performed by minimizing the complex function composed of the maximum temperature difference (MTD) and entropy generation rate (EGR), and the influence of the weighting coefficient (a_0) on the optimal constructral is studied. Secondly, the multi-objective optimization (MOO) with the MTD and EGR as optimization objectives is performed, and the Pareto frontier with an optimal set is obtained by using NSGA-II. The optimization results are selected from the Pareto frontier through LINMAP, TOPSIS, and Shannon Entropy decision methods, and the deviation indexes of different objectives and decision methods are compared. The research of the quadrilateral HGB shows that the optimal constructral can be gained by minimizing the complex function with the objectives of the MTD and the EGR, the complex function after the constructral design is reduced by up to 2% compared with its initial value, and the complex function of the two reflects the compromise between the maximum thermal resistance and the irreversible loss of heat transfer. The Pareto frontier includes the optimization results of different objectives, and when the weighting coefficient of a complex function changes, the optimization results obtained by minimizing the complex function will also be distributed in the Pareto frontier. The deviation index of the TOPSIS decision method is 0.127, which is the lowest one among the discussed decision methods.

Keywords: constructral theory; entropy generation minimization; quadrilateral heat generation body; heat conduction; multi-objective optimization; generalized thermodynamic optimization



Citation: Zhu, H.; Chen, L.; Ge, Y.; Shi, S.; Feng, H. Multi-Objective Constructral Design for Quadrilateral Heat Generation Body with Vein-Shaped High Thermal Conductivity Channel. *Entropy* **2022**, *24*, 1403. <https://doi.org/10.3390/e24101403>

Academic Editors: Mikhail Sheremet and Abderrahmane Bairi

Received: 2 September 2022

Accepted: 27 September 2022

Published: 1 October 2022

Publisher's Note: MDPI stays neutral with regard to jurisdictional claims in published maps and institutional affiliations.



Copyright: © 2022 by the authors. Licensee MDPI, Basel, Switzerland. This article is an open access article distributed under the terms and conditions of the Creative Commons Attribution (CC BY) license (<https://creativecommons.org/licenses/by/4.0/>).

1. Introduction

Arranging high thermal conductivity channels (HTCCs) is a common method to perform the heat dissipation design of electronic devices so that the internal heat can be concentrated and dissipated to the outside through the HTCCs. Therefore, optimizing the arrangement of HTCCs is an important study. Bejan established entropy generation minimization theory [1,2], which measures the performance of the heat transfer process by evaluating the degree of irreversible loss of energy and provides a new evaluation method for thermodynamic optimization. Since the entropy generation minimization theory was proposed, it has been widely used in heat conduction [3–8], fins [9–14], heat exchangers [15–20], and heat sinks [21–26]. The constructral theory [27–29] optimizes problems by following the idea that the structure of things develops in the direction of better internal flow performance, which provides a new method for traditional thermodynamic optimization problems. Constructral theory proved to be fully interdisciplinary and versatile, it can be used in heat transfer problems [30–40], fluid flow problems [36–43], solar cell [44], and stiffened plates [45] designs.

The maximum temperature difference (MTD) is one of the optimization objectives for the constructal design of a heat generation body (HGB). Bejan [30] first performed the constructal design of the two-dimensional rectangular HGB embedded with HTCCs by minimizing the MTD and assembled a new first-level structure according to its optimal constructal. Ghodoossi and Eğrican [46] obtained the optimal constructal of the triangular HGB by minimizing the MTD with the analytical method. da Silva et al. [47] studied the “disc-point” thermal conductivity problem, arranged strip-shaped HTCCs on the circumferential side of the disc HGB, and the optimal constructal by taking MTD as the objective was obtained. Zhang et al. [48] obtained the optimal constructal of arrow-shaped HTCCs in square HGB through a three-degree-of-freedom constructal design, which further reduced the MTD of the square HGB. Hajmohammadi et al. [49] established an annular fin model embedded with HTCCs and obtained the optimal constructal of the HTCCs by minimizing the MTD. According to the common plant leaf veins in nature, Li and Feng [50] proposed a quadrilateral HGB model embedded with vein-shaped HTCCs and obtained its optimal constructal by minimizing the MTD.

The MTD reflects the maximum thermal resistance in the HGB, while the entropy generation rate (EGR) can reflect the irreversible loss of heat transfer in the HGB. Some scholars further studied the EGR performance of different HGBs based on EGR. Ghodoossi [51] studied the optimal constructal of the rectangular HGB by minimizing the MTD and further analyzed the EGR performance of the HGB. Tescari et al. [52] studied the rectangular HGB with the objective of minimizing the EGR and compared it with the optimal constructal obtained by minimizing the MTD. You et al. [53] performed the constructal design of the non-uniform triangular HGB with the objective of the EGR. Feng et al. [54] obtained the optimal constructal of the disc HGB with the objective of the EGR. Ribeiro and Queiros-Condé [55] performed the constructal optimization of the square HGB with I-shaped HTCC, and further analyzed the local EGR performance. Zhu et al. [56] further gained the optimal constructal of the quadrilateral HGB established in Ref. [50] with the minimum EGR. The research showed that the optimal constructal with the minimum EGR is different from that obtained by minimizing the MTD.

The above constructal designs are all single-objective optimizations, which can only meet a single design requirement, but the actual engineering design often needs to meet multiple design requirements. Therefore, the multi-objective optimization (MOO) not only adapts to the engineering design requirements but also promotes the update and replacement of the heat dissipation design strategy of electronic devices. The Non-dominated Sorting Genetic Algorithm II (NSGA-II) [57] with an elite strategy has been successfully applied to many engineering designs [58–69]. In particular, some scholars apply the NSGA-II algorithm to the study of constructal design with different optimization objectives. Chen et al. [70] proposed a non-uniform disc HGB model considering the thermal and flow performance and performed the constructal design by minimizing the complex function with the objectives of the MTD and pumping power consumption (PPC) in the HGB. Zhang et al. [71] obtained the optimal constructal of the trapezoidal HGB with heat conduction and flow by minimizing the complex function with the objectives of the EGR and PPC. Furthermore, the NSGA-II is used to perform MOO on this problem to obtain the Pareto frontier. The research shows that the optimization result with the minimum complex function is distributed in the Pareto frontier. Feng et al. [72] obtained the optimal constructal of marine condensers with single-objective optimization and MOO and compared the optimization results of single-objective optimization and three decision methods based on deviation index. Feng et al. [73] used the NSGA-II to perform the constructal design with the minimum EGR and the constructal design with the minimum PPC and compared the optimization results of three decision methods based on the deviation index.

In this paper, a multi-objective constructal design of the quadrilateral HGB established in Ref. [50] will be performed. Firstly, the constructal design will be performed by minimizing a complex function with the objectives of the MTD and EGR, and the influence of the weighting coefficient (a_0) on the optimal constructal will be studied. Secondly, the

MOO with MTD and EGR as optimization objectives will be performed, and the Pareto frontier with optimal settings will be obtained by using NSGA-II. The optimization results will be selected from the Pareto frontier through LINMAP, TOPSIS, and Shannon Entropy decision methods, and the deviation indexes of different objectives and decision methods will be compared.

2. Model and Optimization Objectives

2.1. Quadrilateral Heat Generation Body Model

Figure 1 shows the quadrilateral HGB model [50]. The quadrilateral HGB (heat generation rate is q''' , thermal conductivity is k_0) is symmetrical about OA, the length of OA is L_1 , the height from point B to OA is H_1 , and the total area is $A_1 = H_1 \times L_1$. The shape of the quadrilateral HGB changes with the aspect ratio H_1/L_1 and the angle θ between BA and OA. A series of branch HTCCs $M_iD_i (i = 1, 2, 3, \dots, n)$ (width is D_0) are equidistantly distributed on the central HTCC (width is D_1), and the central HTCC is divided into n intervals ($n \gg 1$). The point M_i of the branch HTCC is located in the middle of the i th intervals, and $M_iD_i (i = 1, 2, 3, \dots, n)$ is parallel to BA. The thermal conductivity of the HTCC is $k_c \gg k_0$. The periphery of the quadrilateral HGB is adiabatic, and its internal heat is concentrated through HTCCs and dissipated from the point A (temperature is T_0) to the outside.

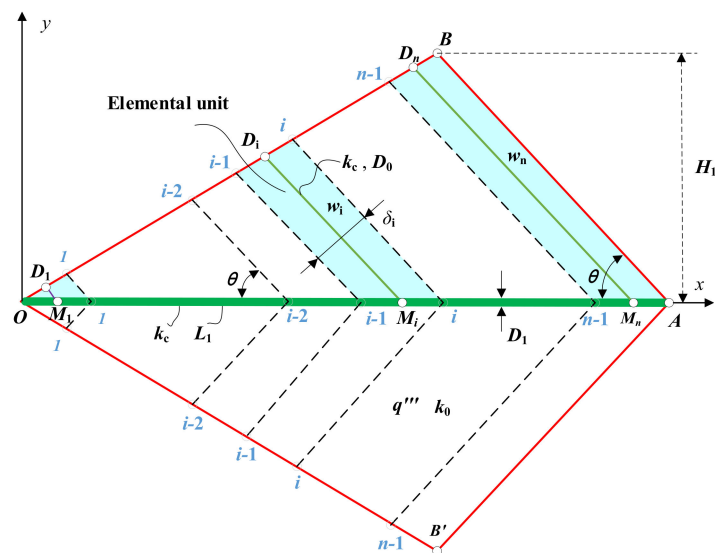


Figure 1. Quadrilateral HGB with vein shaped HTCCs [50].

The elemental unit based on any branch HTCC M_iD_i is shown in Figure 2 [50]. The height of the trapezoidal elemental unit is $\delta_i (\delta_i = (L_1 \sin \theta) / n)$. When $n \gg 1$, $\delta_i \ll w_i$. The trapezoidal “abcd” is similar to rectangular “1234”.

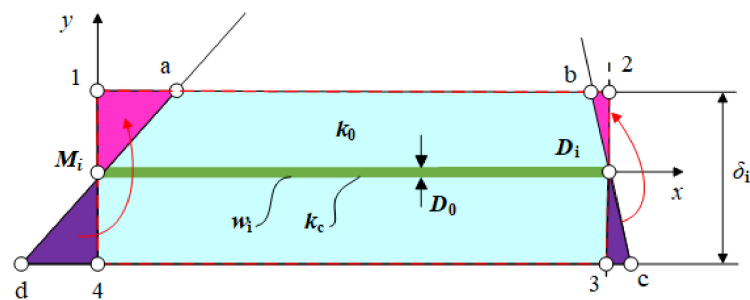


Figure 2. Elemental unit based on any branch HTCC [50].

When $\delta_i \ll w_i$, the heat flow is perpendicular to M_iD_i , and the differential equation can be expressed as:

$$\frac{\partial^2 T}{\partial y^2} + \frac{q'''}{k_0} = 0 \tag{1}$$

The boundary conditions are:

$$\frac{\partial T}{\partial y} = 0, y = \delta_i/2 = L_1 \sin \theta / 2n \tag{2}$$

$$T = T_i(x), y = 0 \tag{3}$$

where $T_i(x)$ is the temperature at the central of M_iD_i .

When $y > 0$, solving Equation (1) yields:

$$T(x, y) = \frac{q'''}{2k_0} \left(\frac{L_1 \sin \theta}{n} y - y^2 \right) + T_i(x) \tag{4}$$

The heat conduction differential equation of the M_iD_i can be expressed as:

$$k_c D_0 \frac{d^2 T_i}{dx^2} + q''' \frac{L_1 \sin \theta}{n} = 0 \tag{5}$$

The boundary conditions are:

$$\frac{dT_i}{dx} = 0, x = w_i = (i - 0.5)H_1 / n \sin \theta \tag{6}$$

$$T_i = T(0, 0) = T_{M_i}, x = 0 \tag{7}$$

Substituting $T_i(x)$ into Equation (4) yields:

$$T(x, y) - T_{M_i} = \frac{q'''}{2k_0} \left(\frac{L_1 \sin \theta}{n} y - y^2 \right) + \frac{q''' L_1 \sin \theta}{2nk_c D_0} \left(\frac{(2i - 1)H_1}{n \sin \theta} x - x^2 \right) \tag{8}$$

The porosity of HTCC in the elemental unit is:

$$\alpha_0 = \frac{D_0 w_i}{\delta_i w_i} = \frac{n D_0}{L_1 \sin \theta} \tag{9}$$

The porosity of the HTCCs of the quadrilateral HGB is:

$$\alpha_1 = \left(2 \sum_{i=1}^n \frac{(i - 0.5) D_0 H_1}{n \sin \theta} + D_1 L_1 \right) / A_1 \tag{10}$$

From Equations (9) and (10), one has:

$$\alpha_1 = \alpha_0 + \frac{D_1}{H_1} \tag{11}$$

2.2. Maximum Temperature Difference

Figure 3 shows the central HTCC [50]. The heat flows to point A from point M_i . The temperature difference distribution between points M_i and M_{i+1} can be obtained as:

$$\frac{\partial^2 T}{\partial x^2} = 0 \tag{12}$$

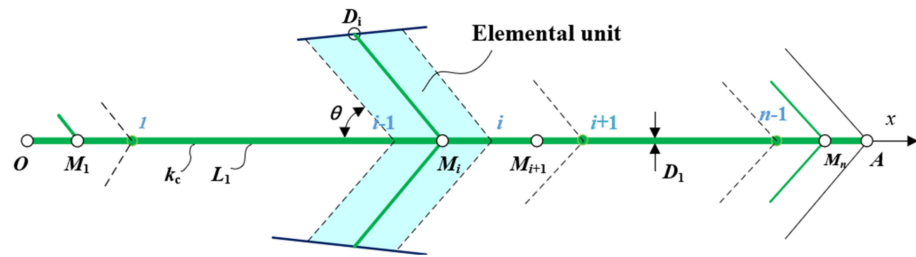


Figure 3. Central HTCC [50].

The boundary conditions are:

$$-k_c D_1 \frac{dT}{dx} = q''' \left(\frac{i}{n}\right)^2 L_1 H_1, x = (i - 0.5)L_1/n(M_i) \tag{13}$$

$$T = T_{M_{i+1}}, x = (i + 0.5)L_1/n(M_{i+1}) \tag{14}$$

From Equations (12)–(14), one has:

$$T - T_{M_{i+1}} = -\frac{q''' i^2 L_1 H_1}{D_1 n^2 k_c} (x - (i + 0.5)L_1/n) \tag{15}$$

Substituting $(i - 0.5)L_1/n$ for x in Equation (15), the temperature difference between M_{i+1} and M_i is:

$$T_{M_i} - T_{M_{i+1}} = \frac{q''' i^2 L_1^2 H_1}{D_1 n^3 k_c} \tag{16}$$

The temperature difference distribution between points M_n and A is:

$$\frac{\partial^2 T}{\partial x^2} = 0 \tag{17}$$

The boundary conditions are:

$$-k_c D_1 \frac{dT}{dx} = q''' \left(\frac{i}{n}\right)^2 L_1 H_1, x = (n - 0.5)L_1/n(M_n) \tag{18}$$

$$T = T_0, x = L_1(A) \tag{19}$$

From Equations (17)–(19), one has:

$$T - T_0 = -\frac{q''' L_1 H_1}{D_1 k_c} (x - L_1) \tag{20}$$

Substituting $(n - 0.5)L_1/n$ for x in Equation (20), the temperature difference between M_n and A is:

$$T_{M_n} - T_0 = \frac{q''' L_1^2 H_1}{2n D_1 k_c} \tag{21}$$

From Equations (8), (16) and (21), the temperature distribution of the elemental unit in the quadrilateral HGB can be obtained as:

$$T(x, y) = \frac{q'''}{2k_0} \left(\frac{L_1 \sin \theta}{n} y - y^2\right) + \frac{q''' L_1 \sin \theta}{2nk_c D_0} \left(\frac{(2i-1)H_1}{n \sin \theta} x - x^2\right) + \sum_{k=i}^n \frac{q''' k^2 L_1^2 H_1}{D_1 n^3 k_c} + \frac{q''' L_1^2 H_1}{2n D_1 k_c} + T_0 \tag{22}$$

According to the Ref. [50], maximum temperature point T_{max} is on the boundary of the elemental unit. Therefore, the MTD can expressed as:

$$\Delta T = T_{max} - T_0 = \frac{(n(n+1)(2n+1)-i(i-1)(2i-1)-3n^2)q''' A_1 L_1}{6(\alpha_1-\alpha_0)k_c n^3 H_1} + \frac{(2i-1)^2 q''' A_1 H_1}{8n^2 k_c \alpha_0 \sin^2 \theta L_1} \tag{23}$$

where T_{max} is obtained by bringing the interval number i of the elemental unit where the maximum temperature point is located into Equation (22).

2.3. Entropy Generation Rate

According to the Ref. [56], the EGRs (σ_{k_0} and σ_{k_c}) of heat generating area and HTCCs area in quadrilateral HGB can be obtained as:

$$\sigma_{k_0} = \iint_{A_{k_0}} k_0 \cdot [(dT/dx)^2 + (dT/dy)^2 / T^2] dA \tag{24}$$

$$\sigma_{k_c} = \iint_{A_{k_c}} k_c \cdot [(dT/dx)^2 + (dT/dy)^2 / T^2] dA \tag{25}$$

where A_{k_0} and A_{k_c} are the areas of heat generating area and HTCCs area in quadrilateral HGB.

The total EGR of quadrilateral HGB can be obtained as:

$$\begin{aligned} \sigma &= \sigma_{k_0} + \sigma_{k_c} \\ &= \frac{q'''^2 A_1^2 L_1}{5(\alpha_1 - \alpha_0)k_c T_0^2 H_1} - \frac{q'''^2 A_1^2 L_1}{30(\alpha_1 - \alpha_0)k_c n^4 T_0^2 H_1} + \frac{\sin^2 \theta q'''^2 A_1^2 L_1}{12k_0 n^2 T_0^2 H_1} + \frac{q'''^2 A_1^2 L_1}{3(\alpha_1 - \alpha_0)k_c n^2 T_0^2 H_1} \\ &\quad + \frac{3q'''^2 A_1^2 L_1}{4(\alpha_1 - \alpha_0)k_c n T_0^2 H_1} + \frac{q'''^2 A_1^2 H_1}{6 \sin^2 \theta \alpha_0 k_c T_0^2 L_1} - \frac{q'''^2 A_1^2 H_1}{12 \sin^2 \theta \alpha_0 k_c n^2 T_0^2 L_1} \end{aligned} \tag{26}$$

3. Multi-Objective Constructal Designs

3.1. Design with a Complex Function

According to the Ref. [50], taking $A_1 = 5 \times 10^3 \text{ mm}^2$, $k_c/k_0 = 470$, $k_0 = 0.8 \text{ W/m} \cdot \text{K}$, $\alpha_1 = 0.15$, $\alpha_0 = \alpha_1/2$, $n = 30$, $T_0 = 297 \text{ K}$ and $q''' = 2 \times 10^4 \text{ W/m}^3$. Figure 4 shows the relationships of ΔT and σ versus H_1/L_1 [50,56]. From Figure 4, $(H_1/L_1)_{T,opt}$ corresponding to the minimum MTD is smaller than the $(H_1/L_1)_{S,opt}$ corresponding to the minimum EGR. σ_T corresponding to the minimum MTD is larger than σ_{min} , and ΔT_S corresponding to the minimum EGR is larger than ΔT_{min} . When H_1/L_1 increases between $(H_1/L_1)_{T,opt}$ and $(H_1/L_1)_{S,opt}$, the σ decreases, while ΔT gradually increases.

The MTD reflects the maximum thermal resistance of the quadrilateral HGB and the EGR reflects the irreversible loss of heat transfer of the quadrilateral HGB. Optimizing the MTD or EGR of the quadrilateral HGB alone cannot fully reflect the comprehensive heat transfer performance of the quadrilateral HGB. Therefore, a complex function composed of the MTD and the EGR based on the linear weighting method [70,71] is established:

$$F_{ST} = a_0 \frac{\Delta T}{\Delta T_{int}} + (1 - a_0) \frac{\sigma}{\sigma_{int}} \tag{27}$$

where a_0 is the weighting coefficient, and $\Delta T_{int}(= 1.77 \text{ K})$ and $\sigma_{int}(= 1.59 \times 10^{-3} \text{ W} \cdot \text{K}^{-1})$ are the MTD and EGR of the HGB under the initial structure, respectively.

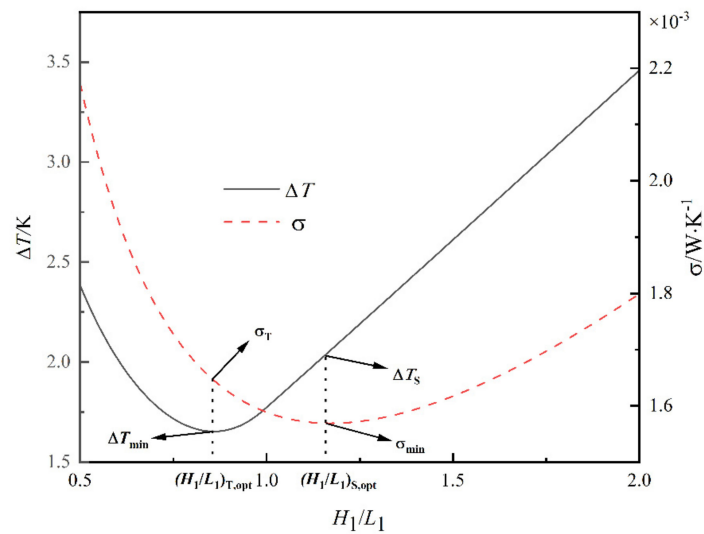


Figure 4. Relationships of ΔT and σ versus H_1/L_1 [50,56].

Figure 5 shows the relationship of F_{ST} versus H_1/L_1 for $a_0 = 0.5$. Figure 6 shows the effects of a_0 on $F_{ST,min}$ and $(H_1/L_1)_{opt}$. From Figure 5, when $a_0 = 0.5$, $(H_1/L_1)_{opt}$ and $F_{ST,min}$ are 0.905 and 0.980, respectively. Compared with the initial structure, F_{ST} , H_1/L_1 and ΔT are reduced by 2.0%, 9.5% and 6.07%, respectively, while σ increased by 2.06%. When H_1/L_1 reaches $(H_1/L_1)_{opt}$, ΔT and σ achieve the best compromise. From Figure 6, when $a_0 = 0$, $(H_1/L_1)_{opt}$ is equal to $(H_1/L_1)_{S,opt}$. When $a_0 = 1$, $(H_1/L_1)_{opt}$ is equal to $(H_1/L_1)_{T,opt}$. when $a_0 = 0.16$, $F_{ST,min} = 1$. The optimal constructal can be gained by minimizing the complex function with the objectives of the MTD and the EGR, which is better than the initial design point. The selection of the weighting coefficient has a great influence on the optimal construct, and the optimal complex function gets smaller as the weighting coefficient of EGR decreases. Therefore, design with a complex function relies on the selection of an appropriate weighting coefficient.

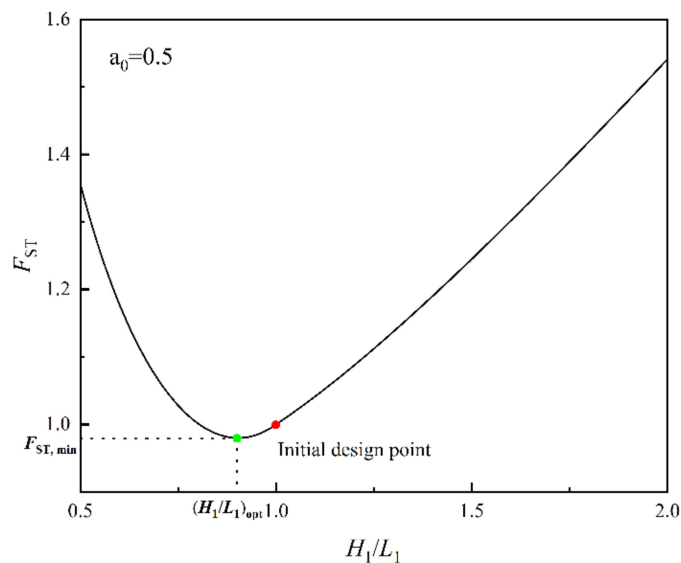


Figure 5. Relationships of F_{ST} versus H_1/L_1 for $a_0 = 0.5$.

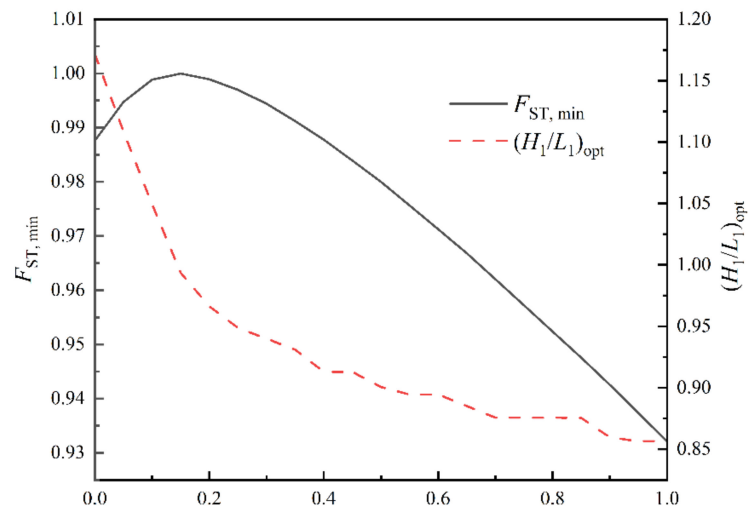


Figure 6. Effects of a_0 on $F_{ST,min}$ and $(H_1/L_1)_{opt}$.

3.2. Design with NSGA-II

In order to adapt the engineering design requirements, The MOO of the quadrilateral HGB is performed by using the “gamultiobj” algorithm that comes from the MATLAB software based on the NSGA-II. Figure 7 shows the complete process of NSGA-II [74]. In the NSGA-II, the decision variable is H_1/L_1 , and the optimization objectives are ΔT and σ . LINMAP, TOPSIS, and Shannon Entropy decision methods [75] are used to select three results from the Pareto frontier that are suitable for the actual needs of the project.

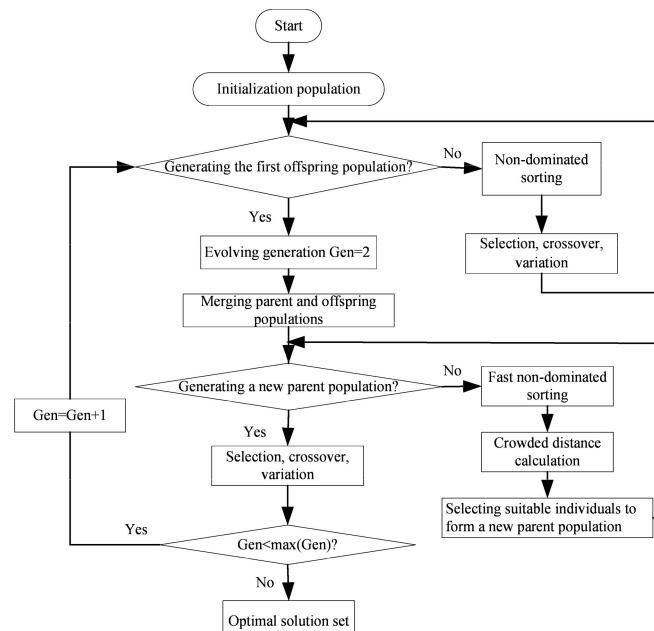


Figure 7. Flow chart of NSGA-II.

Figure 8 shows the Pareto frontier of the dimensionless MTD ($\tilde{\Delta T} = \Delta T / \Delta T_{int}$) and the dimensionless EGR ($\tilde{\sigma} = \sigma / \sigma_{int}$) gained by MOO. From Figure 8, points A and B of the Pareto frontier represent the results of the optimal constructal of the quadrilateral HGB with the minimum $\tilde{\sigma}$ and minimum $\tilde{\Delta T}$, respectively. Although point A and point B correspond to the minimum $\tilde{\sigma}$ and the minimum $\tilde{\Delta T}$, respectively, they also correspond to the maximum $\tilde{\Delta T}$ and the maximum $\tilde{\sigma}$, respectively. Decreasing $\tilde{\sigma}$ (or $\tilde{\Delta T}$) on the Pareto frontier will inevitably lead to $\tilde{\Delta T}$ (or $\tilde{\sigma}$) increase, so it is necessary to find the best com-

promise between $\tilde{\sigma}$ and $\Delta\tilde{T}$ to optimize the comprehensive heat transfer performance of quadrilateral HGB. Point C is an ideal point, which is the minimum point that $\tilde{\sigma}$ and $\Delta\tilde{T}$ can reach. Since the minimum $\tilde{\sigma}$ cannot be obtained when $\Delta\tilde{T}$ reach the minimum point, the ideal point cannot be reached. Point D is a non-ideal point, which is the maximum point that $\tilde{\sigma}$ and $\Delta\tilde{T}$ can reach. Since the maximum $\tilde{\sigma}$ cannot be obtained when $\Delta\tilde{T}$ reach the maximum, the non-ideal point D cannot be reached.

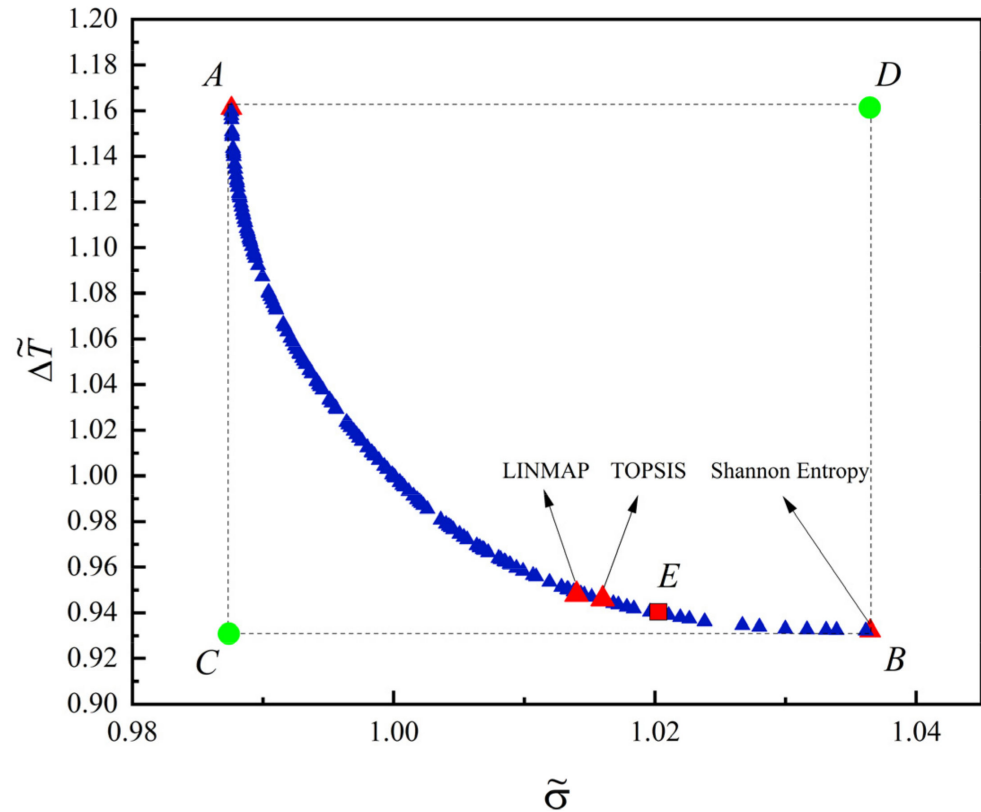


Figure 8. Pareto frontier for multi-objective optimization of the quadrilateral HGB.

Point E is the result of the optimization constructural of the quadrilateral HGB based on the complex function with $\tilde{\sigma}$ and $\Delta\tilde{T}$ as the optimization objective, and point E is an optimal result in the Pareto frontier. When the a_0 of F_{ST} changes, the optimal results of the optimization constructural of the quadrilateral HGB obtained by minimizing the complex function composed of $\tilde{\sigma}$ and $\Delta\tilde{T}$ is also distributed in the Pareto frontier. The remaining optimal results of the Pareto frontier are selected by using other decision methods, and the choice of decision methods needs to be decided by the decision maker according to the actual needs of the project. Therefore, the Pareto frontier can provide a better choice for the performance optimization and constructural design of the quadrilateral HGB.

Figure 9 shows the distribution of H_1/L_1 in the Pareto frontier within its value range. From Figure 9, the two endpoints on the left and right of the abscissa are the lower limit and upper limit of H_1/L_1 in the Pareto frontier, respectively, and the corresponding optimal results are points B and A in Figure 7, respectively. Therefore, individual optimization may not be the substantive optimal result, because the optimal variable is on the boundary of the Pareto frontier.

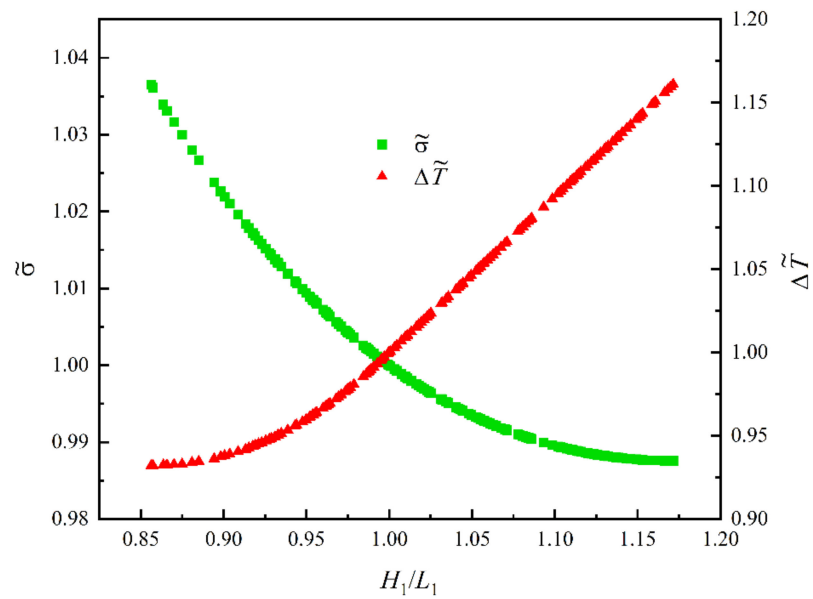


Figure 9. Relationships of $\tilde{\sigma}$ and $\Delta\tilde{T}$ versus H_1/L_1 in Pareto frontier of the quadrilateral HGB.

Table 1 lists the optimization results of different objectives. From Table 1, the optimal result of the Shannon Entropy decision method is the same as that of single-objective optimization with $\tilde{\sigma}$ as optimization objective. The optimal result by minimizing the F_{ST} , and the optimal results obtained through the LINMAP and TOPSIS decision methods are a compromise of the optimal results obtained with the minimum $\tilde{\sigma}$ and minimum $\Delta\tilde{T}$. The constructal design goes through the LINMAP decision methods is similar to that goes through the TOPSIS decision methods, and the corresponding $\Delta\tilde{T}$ decreased by 0.49% and 0.69% compared with the optimal result of F_{ST} , respectively, while the corresponding $\tilde{\sigma}$ increases by 0.75% and 0.96%, respectively. The deviation index [76] of the optimization constructal obtained by TOPSIS decision methods is 0.127, which is better than other decision methods and objectives.

Table 1. Optimization results of the quadrilateral HGB with different objectives.

Optimization Results	Optimization Objectives	$\Delta\tilde{T}$	$\tilde{\sigma}$	F_{ST}	NSGA-II		
					TOPSIS	LINMAP	Shannon Entropy
	$\tilde{\sigma}$	1.036	0.988	1.021	1.016	1.014	1.036
	$\Delta\tilde{T}$	0.932	1.161	0.939	0.946	0.948	0.932
	H_1/L_1	0.857	1.172	0.905	0.923	0.929	0.857
	Deviation indexes [76]	0.175	0.825	0.133	0.127	0.128	0.175

4. Conclusions

Based on the quadrilateral HGB proposed in the previous literature, the multi-objective constructal design is performed. Firstly, the constructal design is performed by minimizing the complex function with the objectives of the MTD and EGR, and the influence on the optimal constructal is studied. Secondly, the MOO with the MTD and EGR as optimization objectives is performed. The optimization results are selected from the Pareto frontier through LINMAP, TOPSIS, and Shannon Entropy decision methods, and the deviation indexes of different objectives and decision methods are compared. The results show:

1. The optimal constructal can be gained by minimizing the complex function with the objectives of the MTD and the EGR. Compared to the initial structure, F_{ST} , H_1/L_1 and ΔT are reduced by 2.0%, 9.5% and 6.07%, respectively, while σ increased by 2.06%. The complex function of the two reflects the compromise between the maximum thermal

- resistance and the irreversible loss of heat transfer. The selection of the weighting coefficient has a great influence on the optimal constructal, and the optimal complex function gets smaller as the weighting coefficient of EGR decreases. Therefore, design with a complex function relies on the selection of an appropriate weighting coefficient.
2. The Pareto frontier includes the optimization results of different objectives, and when the weighting coefficient of complex function changes, the optimization results obtained will also be distributed in the Pareto frontier. The constructal design goes through the LINMAP decision methods is similar to that goes through the TOPSIS decision methods, and the corresponding $\Delta\tilde{T}$ decreased by 0.49% and 0.69% compared with the optimal result of F_{ST} , respectively, while the corresponding $\tilde{\sigma}$ increases by 0.75% and 0.96%, respectively.
 3. The deviation index of the optimization constructal obtained by TOPSIS decision methods is 0.127, which is better than other decision methods and objectives. Compared to the optimal construct with minimum MTD and minimum EGR, the optimal construct obtained by using NSGA-II and decision methods has a smaller deviation index and smaller conflict between the two objectives.
 4. Constructal theory and NSGA-II are powerful tools for comprehensive thermal performance improvements of the high thermal conductivity channels. By increasing the optimization objectives, high thermal conductivity channels can be better used in engineering applications considering multiple design requirements.

Author Contributions: Conceptualization: L.C.; funding acquisition: L.C.; methodology: H.Z. and L.C.; software: S.S., Y.G. and H.F.; validation: S.S. and Y.G.; writing—original draft: H.Z.; writing—review and editing: L.C. All authors have read and agreed to the published version of the manuscript.

Funding: This work is supported by the National Natural Science Foundation of China (Project No. 52171317). and Graduate Innovative Fund of Wuhan Institute of Technology (Project No. CX2021045).

Institutional Review Board Statement: Not applicable.

Informed Consent Statement: Not applicable.

Data Availability Statement: Not applicable.

Acknowledgments: The authors wish to thank the editor and reviewers for their careful, unbiased, and constructive suggestions, which led to this revised manuscript.

Conflicts of Interest: The authors declare no conflict of interest.

Nomenclature

A_1	Area of the quadrilateral volume (m ²)
A_{k_0}	The area of k_0 material of the quadrilateral volume (m ²)
A_{k_c}	The area of k_c material of the quadrilateral volume (m ²)
D_0	Width of branching links (m)
D_1	Width of the central link (m)
H_1	Half-height of quadrilateral volume (m)
k_0	Thermal conductivity of heat generation body (W/m·K)
k_c	Thermal conductivity of high thermal conductivity channel (W/m·K)
L_1	Base length of quadrilateral volume (m)
M_i	Starting point of i th branching link (-)
n	Number of branches of the central high thermal conductivity material (-)

q'''	Heat generation rate per unit volume (W/m^3)
T	Temperature (K)
w_i	Length of i th branching link (m)
F_{ST}	Complex function
a_0	Weighting coefficient
Greek symbols	
α	Porosity of thermal conductivity channel (-)
θ	Angle defined in Figure 1 (rad)
δ_i	Height of i th branching link (m)
σ	Entropy generation rate ($W/m \cdot K$)
Superscript	
\sim	Dimensionless
Subscripts	
i	Counting index
opt	Optimum
min	Minimum
Abbreviations	
HGB	Heat generation body
HTCC	High thermal conductivity channel
MTD	Maximum temperature difference
EGR	Entropy generation rate
MOO	Multi-objective optimization
PPC	Pumping power consumption

References

1. Bejan, A. *Entropy Generation through Heat and Fluid Flow*; Wiley: New York, NY, USA, 1982.
2. Bejan, A. *Entropy Generation Minimization*; CRC Press: Boca Raton, FL, USA, 1996.
3. Sahin, A.Z. Entropy production minimization in steady state heat conduction. *Int. J. Phys. Sci.* **2011**, *6*, 2826–2831.
4. Sahin, A.Z. Critical insulation thickness for maximum entropy generation. *Int. J. Exergy* **2012**, *9*, 34–43. [[CrossRef](#)]
5. Morriss, G.P.; Truant, D.P. Dissipation and entropy production in deterministic heat conduction of quasideimensional systems. *Phys. Rev. E* **2013**, *86*, 062144. [[CrossRef](#)] [[PubMed](#)]
6. Ebrahimi, A.; Rikhtegar, F.; Sabaghan, A.; Roohi, E. Heat transfer and entropy generation in a microchannel with longitudinal vortex generators using nanofluids. *Energy* **2016**, *101*, 191–201. [[CrossRef](#)]
7. Tian, X.W.; Wang, L.Q. Heat conduction in cylinders: Entropy generation and mathematical inequalities. *Int. J. Heat Mass Transfer* **2018**, *121*, 1137–1145. [[CrossRef](#)]
8. Mansoor, S.B.; Yilbas, B.S. Entropy generation rate for stationary ballistic-diffusive heat conduction in a rectangular flake. *J. Comput. Theor. Trans.* **2021**, *50*, 87–101. [[CrossRef](#)]
9. Aziz, A.; Khan, W.A. Minimum entropy generation design of a convectively heated pin fin with tip heat loss. *Int. J. Exergy* **2012**, *9*, 44–60. [[CrossRef](#)]
10. Moghaddam, A.J.; Saedodin, S. Entropy generation minimization of pin fin heat sinks by means of metaheuristic methods. *Indian J. Sci. Technol.* **2013**, *6*, 4886–4893. [[CrossRef](#)]
11. Khatami, S.; Rahbar, N. An analytical study of entropy generation in rectangular natural convective porous fins. *Therm. Sci. Eng. Prog.* **2019**, *11*, 142–149. [[CrossRef](#)]
12. Bhat, P.; Katte, S.S. Entropy analysis of a simple rectangular radiating fin for space applications. *Int. J. Heat Technol.* **2020**, *28*, 708–714. [[CrossRef](#)]
13. Hazarika, S.A.; Bhanja, D.; Nath, S. Fork-shaped constructal fin array design a better alternative for heat and mass transfer augmentation under dry, partially wet and fully wet conditions. *Int. J. Therm. Sci.* **2020**, *152*, 106329. [[CrossRef](#)]
14. Giorgi, C.; Zull, F. Entropy rates and efficiency of convecting-radiating fins. *Energies* **2021**, *14*, 1643. [[CrossRef](#)]
15. Farzaneh-Gord, M.; Ameri, H.; Arabkoohsar, A. Tube-in-tube helical heat exchangers performance optimization by entropy generation minimization approach. *Appl. Therm. Eng.* **2016**, *108*, 1279–1287. [[CrossRef](#)]
16. Ebrahimi-Moghadam, A.; Moghadam, A.J. Optimal design of geometrical parameters and flow characteristics for Al₂O₃/water nanofluid inside corrugated heat exchangers by using entropy generation minimization and genetic algorithm methods. *Appl. Therm. Eng.* **2019**, *149*, 889–898. [[CrossRef](#)]
17. Liu, J.X.; Jiang, Y.K.; Wang, B.Z.; He, S.M. Assessment and optimization assistance of entropy generation to air-side comprehensive performance of fin-and-flat tube heat exchanger. *Int. J. Therm. Sci.* **2019**, *138*, 61–74. [[CrossRef](#)]
18. Zhang, K.Z.; Liu, M.; Zhao, Y.L.; Wang, C.Y.; Yan, J.J. Entropy generation versus transition time of heat exchanger during transient processes. *Energy* **2020**, *200*, 117490. [[CrossRef](#)]
19. Cao, X.; Zhang, R.Q.; Chen, D.M.; Chen, L.; Du, T.T.; Yu, H. Performance investigation and multi-objective optimization of helical baffle heat exchangers based on thermodynamic and economic analyses. *Int. J. Heat Mass Transfer* **2021**, *176*, 121489. [[CrossRef](#)]

20. Naik, H.; Tiwari, S. Thermodynamic performance analysis of an inline fin-tube heat exchanger in presence of rectangular winglet pairs. *Int. J. Mech. Sci.* **2021**, *193*, 106148. [[CrossRef](#)]
21. Xia, G.D.; Liu, R.; Wang, J.; Du, M. The characteristics of convective heat transfer in microchannel heat sinks using Al₂O₃ and TiO₂ nanofluids. *Int. Commun. Heat Mass Transfer* **2016**, *76*, 256–264. [[CrossRef](#)]
22. Lorenzini, G.; Mahian, O. Entropy in Nanofluids. *Entropy* **2018**, *20*, 339. [[CrossRef](#)] [[PubMed](#)]
23. Kurnia, J.C.; Lim, D.C.; Chen, L.J.; Sasmito, A.P. Entropy generation and heat transfer performance in microchannel cooling. *Entropy* **2019**, *21*, 191. [[CrossRef](#)] [[PubMed](#)]
24. Chauhan, P.R.; Kumar, R.; Bharj, R.S. Optimization of the circular microchannel heat sink under viscous heating effect using entropy generation minimization method. *Therm. Sci. Eng. Prog.* **2019**, *13*, 100365. [[CrossRef](#)]
25. Rasam, H.; Roy, P.; Savoldi, L.; Ghahremanian, S. Numerical assessment of heat transfer and entropy generation of a porous metal heat sink for electronic cooling applications. *Energies* **2020**, *13*, 3851. [[CrossRef](#)]
26. Shahsavari, A.; Yari, O.; Askari, I.B. The entropy generation analysis of forward and backward laminar water flow in a plate-pin-fin heatsink considering three different splitters. *Int. Commun. Heat Mass Transfer* **2021**, *120*, 105026. [[CrossRef](#)]
27. Bejan, A.; Lorente, S. *Design with Constructal Theory*; Wiley: Hoboken, NJ, USA, 2008.
28. Chen, L.G.; Feng, H.J.; Xie, Z.H.; Sun, F.R. Progress of constructal theory in China over the past decade. *Int. J. Heat Mass Transfer* **2019**, *130*, 393–419. [[CrossRef](#)]
29. Bejan, A. *Time and Beauty: Why Time Flies and Beauty Never Dies*; World Scientific: Singapore, 2022.
30. Bejan, A. Constructal-theory network of conducting paths for cooling a heat generating volume. *Int. J. Heat Mass Transfer* **1997**, *40*, 799–816. [[CrossRef](#)]
31. Hajmohammadi, M.R.; Joneydi Shariatzadeh, O.; Moulod, M.; Nourazar, S.S. Phi and Psi shaped conductive routes for improved cooling in a heat generating piece. *Int. J. Therm. Sci.* **2014**, *77*, 66–74. [[CrossRef](#)]
32. Hajmohammadi, M.R.; Parsa, H.; Najafian, J. Proposing an optimal tree-like design of highly conductive material configuration with unequal branches for maximum cooling a heat generating piece. *Int. J. Heat Mass Transfer* **2019**, *142*, 118422. [[CrossRef](#)]
33. Hajmohammadi, M.R.; Rezaei, E. Proposing a new algorithm for the optimization of conduction pathways based on a recursive localization. *Appl. Therm. Eng.* **2019**, *151*, 146–153. [[CrossRef](#)]
34. Chen, L.G.; Wu, W.J.; Feng, H.J. *Constructal Design for Heat Conduction*; Book Publisher International: London, UK, 2021.
35. Bejan, A. *Heat Transfer: Evolution, Design and Performance*; John Wiley & Sons: New York, NY, USA, 2022.
36. Hajmohammadi, M.R.; Shirani, E.; Salimpour, M.R.; Campo, A. Constructal placement of unequal heat sources on a plate cooled by laminar forced convection. *Int. J. Therm. Sci.* **2012**, *60*, 13–22. [[CrossRef](#)]
37. Hajmohammadi, M.R.; Poozesh, S.; Campo, A.; Nourazar, S.S. Valuable reconsideration in the constructal design of cavities. *Energy Convers. Manag.* **2013**, *66*, 33–40. [[CrossRef](#)]
38. Chen, L.G.; Yang, A.B.; Feng, H.J.; Ge, Y.L.; Xia, S.J. Constructal design progress for eight types of heat sinks. *Sci. China Tech. Sci.* **2020**, *63*, 879–911. [[CrossRef](#)]
39. De Lima, Y.T.B.; Mateus das Neves Gomes, M.; Isoldi, L.A.; dos Santos, E.D.; Lorenzini, G.; Rocha, L.A.O. Geometric analysis through the constructal design of a sea wave energy converter with several coupled hydropneumatic chambers considering the oscillating water column operating principle. *Appl. Sci.* **2021**, *11*, 8630. [[CrossRef](#)]
40. Bejan, A. Evolutionary design: Heat and fluid flow together. *Int. Commun. Heat Mass Transfer* **2022**, *132*, 105924. [[CrossRef](#)]
41. Bejan, A. Boundary layers from constructal law. *Int. Commun. Heat Mass Transfer* **2020**, *117*, 102672. [[CrossRef](#)]
42. Lorente, S. Vascular systems for the thermal and hygric management. *Adv. Heat Transfer* **2021**, *53*, 159–185.
43. Bilal, S.; Rehman, M.; Noeiaghdam, S.; Ahmad, H.; Akgül, A. Numerical analysis of natural convection driven flow of a non-Newtonian power-law fluid in a trapezoidal enclosure with a U-shaped constructal. *Energies* **2021**, *14*, 5355. [[CrossRef](#)]
44. Ojeda, J.A.; Messina, S.; Vázquez, E.E.; Méndez, F. Geometry optimization of top metallic contacts in a solar cell using the constructal design method. *Energies* **2020**, *13*, 3349. [[CrossRef](#)]
45. Pinto, V.T.; Rocha, L.A.O.; dos Santos, E.D.; Isoldi, L.A. Numerical analysis of stiffened plates subjected to transverse uniform load through the constructal design method. *Eng. Sol. Mech.* **2022**, *10*, 99–108. [[CrossRef](#)]
46. Ghodoossi, L.; Eğrican, N. Conductive cooling of triangular shaped electronics using constructal theory. *Energy Convers. Manag.* **2004**, *45*, 811–828. [[CrossRef](#)]
47. Da Silva, A.K.; Vasile, C.; Bejan, A. Discs cooled with high-conductivity inserts that extend inward from the perimeter. *Int. J. Heat Mass Transfer* **2004**, *47*, 4257–4263. [[CrossRef](#)]
48. Zhang, F.Y.; Feng, H.J.; Chen, L.G.; You, J.; Xie, Z.H. Constructal design of an arrow-shaped high thermal conductivity channel in a square heat generation body. *Entropy* **2020**, *22*, 475. [[CrossRef](#)]
49. Hajmohammadi, M.R.; Rasouli, E.; Elmi, M.A. Geometric optimization of a highly conductive insert intruding an annular fin. *Int. J. Heat Mass Transfer* **2020**, *146*, 118910. [[CrossRef](#)]
50. Li, Y.L.; Feng, M.L. Optimal design of conductive natural branched pathways for cooling a heat-generating volume. *Heat Transfer* **2021**, *50*, 2571–2591. [[CrossRef](#)]
51. Ghodoossi, L. Entropy generation rate in uniform heat generating area cooled by conducting paths: Criterion for rating the performance of constructal designs. *Energy Convers. Manag.* **2004**, *45*, 2951–2969. [[CrossRef](#)]
52. Tescari, S.; Mazet, N.; Neveu, P. Constructal theory through thermodynamics of irreversible processes framework. *Energy Convers. Manag.* **2011**, *52*, 3176–3188. [[CrossRef](#)]

53. You, J.; Feng, H.J.; Chen, L.G.; Xie, Z.H. Constructal design of nonuniform heat generating area based on triangular elements: A case of entropy generation minimization. *Int. J. Therm. Sci.* **2019**, *139*, 403–412. [[CrossRef](#)]
54. Feng, H.J.; You, J.; Chen, L.G.; Ge, Y.L.; Xia, S.J. Constructal design of a non-uniform heat generating disc based on entropy generation minimization. *Eur. Phys. J. Plus* **2020**, *135*, 257. [[CrossRef](#)]
55. Ribeiro, P.; Queiros-Condé, D. On the entropy production of the elemental construct of the constructal designed plate generating heat. *Int. J. Therm. Sci.* **2019**, *145*, 106043. [[CrossRef](#)]
56. Zhu, H.W.; Chen, L.G.; Ge, Y.L.; Feng, H.J. Constructal entropy generation rate minimization of heat conduction for leaf-shaped quadrilateral heat generation body. *Eur. Phys. J. Plus* **2022**, *137*, 275. [[CrossRef](#)]
57. Deb, K.; Pratap, A.; Agarwal, S.; Meyarivan, T. A fast and elitist multiobjective genetic algorithm: NSGA-II. *IEEE Trans. Evol. Comput.* **2002**, *6*, 182–197. [[CrossRef](#)]
58. Li, Y.; Liao, S.; Liu, G. Thermo-economic multi-objective optimization for a solar-dish Brayton system using NSGA-II and decision making. *Int. J. Electr. Power Energy Syst.* **2015**, *64*, 167–175. [[CrossRef](#)]
59. Fergani, Z.; Morosuk, T.; Touil, D. Exergy-based multi-objective optimization of an organic Rankine cycle with a zeotropic mixture. *Entropy* **2021**, *23*, 954. [[CrossRef](#)]
60. Teng, S.; Feng, Y.Q.; Hung, T.C.; Xi, H. Multi-objective optimization and fluid selection of different cogeneration of heat and power systems based on organic Rankine cycle. *Energies* **2021**, *14*, 4967. [[CrossRef](#)]
61. Baghernejad, A.; Anvari-Moghaddam, A. Exergoeconomic and environmental analysis and Multi-objective optimization of a new regenerative gas turbine combined cycle. *Appl. Sci.* **2021**, *11*, 11554. [[CrossRef](#)]
62. Xie, T.; Xia, S.; Wang, C. Multi-objective optimization of Braun-type exothermic reactor for ammonia synthesis. *Entropy* **2022**, *24*, 52. [[CrossRef](#)]
63. Arora, R.; Kaushik, S.C.; Kumar, R.; Arora, R. Multi-objective thermo-economic optimization of solar parabolic dish Stirling heat engine with regenerative losses using NSGA-II and decision making. *Int. J. Electr. Power Energy Syst.* **2015**, *74*, 25–35. [[CrossRef](#)]
64. Li, R.J.; Grosu, L.; Queiros-Condé, D. Multi-objective optimization of Stirling engine using finite physical dimensions thermodynamics (FPDT) method. *Energy Convers. Manag.* **2016**, *124*, 517–527. [[CrossRef](#)]
65. Patel, V.; Savsani, V.; Mudgal, A. Many-objective thermodynamic optimization of Stirling heat engine. *Energy* **2017**, *125*, 629–642. [[CrossRef](#)]
66. Dai, D.D.; Yuan, F.; Long, R.; Liu, Z.C.; Liu, W. Performance analysis and multi-objective optimization of a Stirling engine based on MOPSOCD. *Int. J. Therm. Sci.* **2018**, *124*, 399–406. [[CrossRef](#)]
67. Nazemzadegan, M.R.; Kasaeian, A.; Toghyani, S.; Ming, T.Z. Multi-objective optimization in a finite time thermodynamic method for dish-Stirling by branch and bound method and MOPSO algorithm. *Front Energy* **2020**, *14*, 649–665. [[CrossRef](#)]
68. Rostami, M.; Assareh, E.; Moltames, R.; Jafarinejad, T. Thermo-economic analysis and multi-objective optimization of a solar dish Stirling engine. *Energy Sources Part A* **2021**, *43*, 2861–2877. [[CrossRef](#)]
69. Shah, P.; Saliya, P.; Raja, B.; Patel, V. A multiobjective thermodynamic optimization of a nanoscale Stirling engine operated with Maxwell-Boltzmann gas. *Heat Tran. Asian. Res.* **2019**, *48*, 1913–1932. [[CrossRef](#)]
70. Chen, C.; You, J.; Feng, H.J.; Chen, L.G. A multi-objective study on the constructal design of non-uniform heat generating disc cooled by radial- and dendritic-pattern cooling channels. *Sci. China Tech. Sci.* **2020**, *64*, 729–744. [[CrossRef](#)]
71. Zhang, Z.M.; Feng, H.J.; Chen, L.G.; Ge, Y.L. Multi-objective constructal design for compound heat dissipation channels in a three-dimensional trapezoidal heat generation body. *Int. Commun. Heat Mass Transfer* **2021**, *127*, 105584. [[CrossRef](#)]
72. Feng, H.J.; Tang, W.; Chen, L.G.; Shi, J.C.; Wu, Z.X. Multi-objective constructal optimization for marine condensers. *Energies* **2021**, *14*, 5545. [[CrossRef](#)]
73. Feng, H.J.; Chen, L.G.; Xie, Z.J.; Tang, W.; Ge, Y.L. Multi-objective constructal design for a marine boiler considering entropy generation rate and power consumption. *Energy Rep.* **2022**, *8*, 1519–1527. [[CrossRef](#)]
74. Li, Y.Y.; Wang, S.Q.; Duan, X.B.; Liu, S.J.; Liu, J.P.; Hu, S. Multi-objective energy management for Atkinson cycle engine and series hybrid electric vehicle based on evolutionary NSGA-II algorithm using digital twins. *Energy Convers. Manag.* **2021**, *230*, 113788. [[CrossRef](#)]
75. Wang, L.B.; Bu, X.B.; Li, H.S. Multi-objective optimization and off-design evaluation of organic Rankine cycle (ORC) for low-grade waste heat recovery. *Energy* **2020**, *203*, 117809. [[CrossRef](#)]
76. Arora, R.; Kaushik, S.C.; Kumar, R.; Arora, R. Soft computing based multi-objective optimization of Brayton cycle power plant with isothermal heat addition using evolutionary algorithm and decision making. *Appl. Soft Comput.* **2016**, *46*, 267–283. [[CrossRef](#)]